

Boosting viscosity sensitivity of magnetic particle imaging using selection field gradients

Cite as: Appl. Phys. Lett. **125**, 242405 (2024); doi: [10.1063/5.0232365](https://doi.org/10.1063/5.0232365)

Submitted: 7 August 2024 · Accepted: 28 November 2024 ·

Published Online: 11 December 2024



View Online



Export Citation



CrossMark

A. Topcu,^{1,2,a)}  A. Alpman,^{1,2,3}  M. Utkur,^{1,2,4}  and E. U. Saritas^{1,2,a)} 

AFFILIATIONS

¹Department of Electrical and Electronics Engineering, Bilkent University, Ankara 06800, Turkey

²National Magnetic Resonance Research Center (UMRAM), Bilkent University, Ankara 06800, Turkey

³Department of Electrical Engineering and Computer Sciences, University of California, Berkeley, California 94720, USA

⁴Boston Children's Hospital, Harvard Medical School, Boston, Massachusetts 02115, USA

^{a)}Authors to whom correspondence should be addressed: atakan.topcu@bilkent.edu.tr and saritas@ee.bilkent.edu.tr

ABSTRACT

In magnetic particle imaging (MPI), selection field (SF) gradients are utilized to form a field-free point (FFP) in space, such that only the magnetic nanoparticles (MNPs) in the vicinity of the FFP respond to the applied drive field (DF) and contribute to the received signal. While the relaxation behavior of MNPs adversely affects image quality by reducing signal intensity and causing blurring, it also provides MPI with functional imaging capabilities, such as viscosity and temperature mapping. This work investigates the effects of SF gradients on the relaxation behavior of the MNPs using an in-house magnetic particle spectrometer (MPS) setup equipped with an additional DC electromagnet SF coil, which switches the MPS setup into an MPI system. The results reveal that the presence of SF gradients boosts the viscosity sensitivity of MPI, and that the MPI signal can be sensitized to viscosity even at high DF frequencies and amplitudes if sufficiently large SF gradients are applied.

Published under an exclusive license by AIP Publishing. <https://doi.org/10.1063/5.0232365>

Magnetic particle imaging (MPI) utilizes magnetic nanoparticles (MNPs) as tracers to quantitatively image their spatial distribution with high sensitivity and without any signal from the background tissue.^{1,2} In MPI, selection field (SF) coils are used to generate static magnetic field gradients that form a field-free point (FFP) in space. Due to the nonlinear magnetization response of MNPs, only the MNPs in the vicinity of the FFP have unsaturated magnetization and contribute to the signal induced on the receive coil. Then, an additional oscillating magnetic field called drive field (DF) is applied to sweep the FFP in space. In practice, the magnetic moments of MNPs cannot align with the DF instantaneously due to their relaxation behavior. The resulting delayed response reduces the signal intensity and causes blurring in the image.^{3,4} Despite such disadvantages, relaxation phenomenon also grants functional imaging capabilities to MPI, such as temperature mapping,^{5–7} viscosity mapping,^{7,8} and differentiating different MNP types.^{9,10}

Certain diseases such as cancer¹¹ and atherosclerosis¹² are known to cause locally increased cellular viscosity levels. The relaxation behavior of MNPs enables MPI to probe the viscosity of the tissue in which the MNPs are located, providing a promising tool for the diagnosis of these diseases. Previous work in the literature has investigated the

potential of MPI for viscosity mapping using magnetic particle spectrometer (MPS) setups^{7,13–15} and MPI imaging systems.^{8,16,17} In comparison to MPI imaging experiments, MPS measurements are typically orders of magnitude faster to acquire and exhibit significantly higher signal-to-noise ratio (SNR). This enhanced efficiency facilitates rapid characterization of MNPs across various experimental conditions. Moreover, MPS measurements help to predict the performance of MNPs in MPI systems. However, previous work has shown that the relaxation dynamics of MNPs shows subtle differences in an MPS setup vs an MPI system, displaying comparable trends but at different frequencies.⁸ Understanding the differences between the MNP dynamics in these two systems is crucial to fully realize the noninvasive *in vivo* viscosity mapping potential of MPI.

In this study, we investigate the effects of magnetic field gradients on the relaxation behavior of MNPs using an in-house arbitrary-waveform (AW) MPS setup equipped with an additional DC electromagnet SF coil that switches the MPS setup into an MPI system. We present MPS-to-MPI transition results for SF gradients ranging between 0 and 1.1 T/m and for viscosity levels in the biologically relevant range of up to 6.9 mPa.s. We demonstrate the effects of the SF gradients on the relaxation time constant (τ) of the MNPs using a time constant

estimation technique called TAURUS (TAU estimation via Recovery of Underlying mirror Symmetry).^{4,18} The results show that SF gradients enhance the viscosity sensitivity of MPI, i.e., they improve the ability of the MNP response to capture and reflect changes in viscosity. The results also demonstrate that a stronger SF gradient is needed to sensitize the signal to viscosity at higher DF frequencies and amplitudes.

Using Faraday's law of induction, the received signal in MPI can be expressed as follows:^{19,20}

$$s(t) = -\mu_0 \int_V \mathbf{B}_{\text{rec}}(\mathbf{r}) \cdot c(\mathbf{r}) \frac{\partial \bar{\mathbf{m}}(\mathbf{H}(\mathbf{r}, t))}{\partial t} dV. \quad (1)$$

Here, $\mathbf{B}_{\text{rec}}(\mathbf{r})$ is the position-dependent receive coil sensitivity vector, $\mathbf{H}(\mathbf{r}, t)$ is the applied external field vector, $c(\mathbf{r})$ is the MNP concentration, and $\bar{\mathbf{m}}$ is the average magnetic dipole moment of MNPs. In the adiabatic case, where the magnetic moments of the MNPs align instantaneously with the applied field, the MNP magnetization is typically described by the Langevin function as

$$\bar{\mathbf{m}}(\mathbf{H}(\mathbf{r}, t)) = m \mathcal{L}(k\mathbf{H}(\mathbf{r}, t)) \hat{\mathbf{H}}(\mathbf{r}, t), \quad (2)$$

where $\mathcal{L}(\cdot)$ is the Langevin function, $\hat{\mathbf{H}}$ is the unit vector along the direction of \mathbf{H} , m is the magnetic moment of a single MNP, and k is an MNP parameter that depends on m and temperature. However, the adiabatic approximation no longer applies when the applied field changes rapidly, as in the case of MPI. In such cases, the magnetic moments of MNPs lag behind the external field, while following a combination of external physical rotation (Brownian relaxation) and internal magnetization rotation (Néel relaxation) of the MNPs.^{21,22} Among these two relaxation processes, only the Brownian relaxation depends on the viscosity of the medium, whereas both the Brownian and Néel relaxations depend on the temperature of the medium.

The relaxation process in the presence of an oscillating magnetic field is an active topic of interest in MPI, as the Brownian and Néel mechanisms are defined under zero-field conditions. In one of the practical approaches, the effective relaxation process under a sinusoidal DF has been modeled as a first-order Debye process, resulting in the following signal equation:³

$$s(t) = s_{\text{adiabatic}}(t) * \left\{ \frac{1}{\tau} e^{-\frac{t}{\tau}} u(t) \right\}. \quad (3)$$

Here, τ is the effective relaxation time constant, $u(t)$ is the Heaviside step function, and “*” denotes the convolution operation. This signal equation indicates that the relaxation process simultaneously reduces the signal intensity and causes a lag in the time-domain signal.

A previously proposed technique called TAURUS estimates τ directly from the time-domain signal, without requiring any prior information about the MNPs. Accordingly, τ is computed in frequency-domain as follows:^{4,8}

$$\tau(f) = \frac{S_{\text{pos}}^*(f) + S_{\text{neg}}(f)}{i2\pi f (S_{\text{pos}}^*(f) - S_{\text{neg}}(f))}. \quad (4)$$

Here, $S_{\text{neg}}(f)$ and $S_{\text{pos}}(f)$ are the respective Fourier transforms of the positive and negative half cycles of $s(t)$ acquired under a sinusoidal DF, and the superscript “*” denotes the complex conjugation operation. In the ideal case, this frequency-domain computation should

yield the same $\tau(f)$ at all frequencies. However, deviations from the model in Eq. (3) as well as noise and interferences make the result frequency dependent. For robust τ estimation, we cast this equation as a weighted least squares (WLS) problem and compute a single τ value for $s(t)$ via WLS regression in frequency domain.¹⁰

In this work, we performed experiments on our in-house AW MPS setup featuring a DC electromagnet SF coil (see Fig. 1) to investigate how τ is affected by the presence of SF gradients. The DF coil had a relatively low inductance of 13.3 μH , allowing flexible selection of DF frequency without the need for impedance matching.^{23,24} The DF coil efficiency was measured as 0.664 mT/A along the z -direction using a Gaussmeter (LakeShore, 475 DSP). A tunable two-section gradiometric receive coil was utilized to decouple the drive and receive coils, and its cancellation section was manually adjusted before the experiments to minimize the direct feedthrough interference. The self-resonance of the receive coil was around 320 kHz. The receive chamber had a maximum size of 0.7 cm in diameter and 1 cm in height. A power amplifier (AE Techron 7224) was utilized to amplify the DF waveform, and a Rogowski current probe (LFR 06/6/300, PEM Ltd.) was used for real-time observation of the DF waveform. The received signal was band-pass filtered between 300 Hz and 300 kHz and amplified using a low-noise pre-amplifier (SRS SR560) before digitization via a data acquisition card (NI-PCIe 6374). The direct feedthrough interference was further digitally canceled by subtracting an empty chamber measurement from the measured MNP signal. The fundamental harmonic was filtered out using a digital high-pass filter with $1.5f_0$ cutoff frequency, where f_0 is the DF frequency.

As shown in Fig. 1, SF gradients were generated in the receive chamber using a DC electromagnet composed of two coils in Maxwell configuration, each with 11 layers and 22 turns per layer, wound using a 1.2 mm diameter copper wire. A 3D-printed structure was prepared for housing the MPS setup in a fixed position while ensuring accurate positioning of the SF coil with respect to the MPS setup. The SF coil efficiency was calculated via MATLAB simulations and validated experimentally using axial and transverse probes of a Hall effect Gaussmeter (LakeShore 475 DSP) mounted on a three-axis robotic arm (Velmex BiSlide). Measurements were performed within a $1 \times 1 \times 1 \text{ cm}^3$ volume encompassing the receive chamber, with 1 A DC passing through the SF coil. As shown in Fig. 1(d), the SF gradient efficiency was $(-0.16, 0.08, \text{ and } 0.08) \text{ T/m/A}$ in (x, y, z) directions. A maximum SF gradient of $G = 1.1 \text{ T/m}$ in the x -direction was achieved within the hardware limits, which is comparable to those in some of the preclinical MPI systems utilized in the literature.^{25,26} The SF gradient within the receive chamber had greater than 98% homogeneity. The SF coil was air-cooled to maintain a constant temperature within the measurement chamber.

For the experiments, DF at five different frequencies between $f_0 = 1$ and 5 kHz and five different amplitudes between $B_p = 7.5$ and 17.5 mT were applied, resulting in 25 different operating points (OPs). The OPs were arranged into two separate groups as shown in Fig. 2(a), so that the expected peak signal amplitudes within each group varied by at most threefold. This arrangement ensured that the maximum pre-amplifier gain can be applied for each group. The DF waveform at each OP consisted of 40 periods followed by a gap of matching duration to avoid transient effects between different OPs [see Fig. 2(b)]. All measurements were repeated three times. For each repetition, a new empty chamber baseline measurement was performed, and the 25 OPs

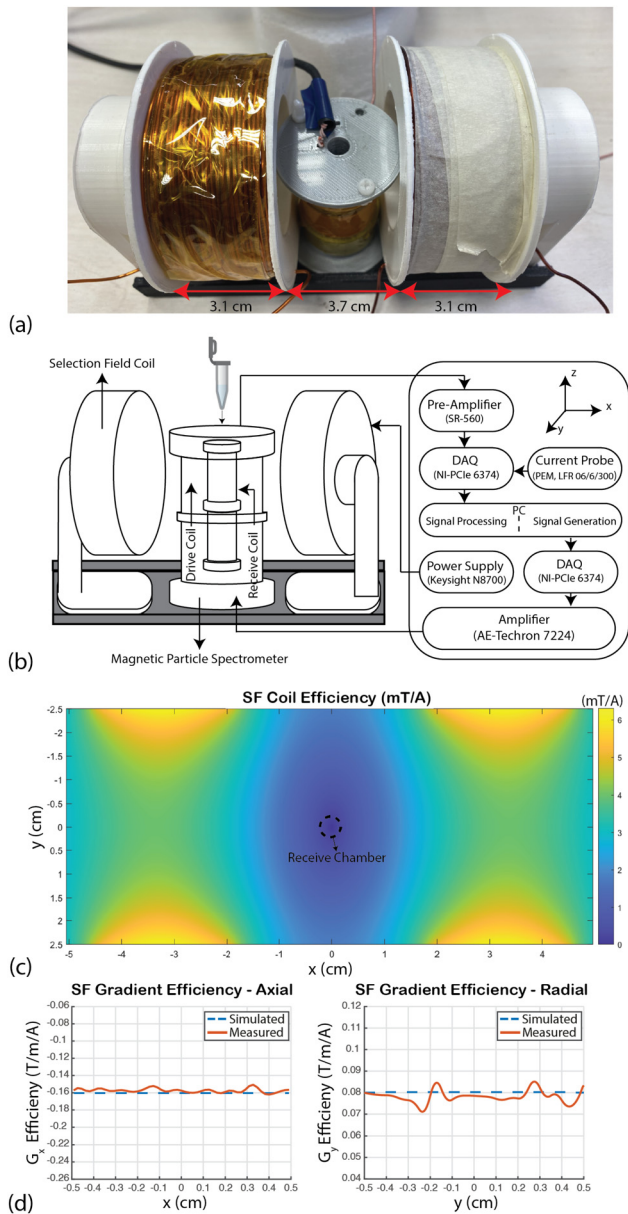


FIG. 1. (a) Our in-house arbitrary-waveform MPS setup equipped with a DC electromagnet SF coil. The drive and receive coils were placed coaxially along the z-direction. The SF coil, composed of two coils in Maxwell configuration, was positioned along the x-axis and provided magnetic field gradients along all three axes. (b) Schematic of the experimental setup and the transmit/receive chain workflow. (c) Simulated efficiency map for SF coil, generating up to 1.1 T/m magnetic field gradient in the x-direction, within the receive chamber. (d) SF gradient efficiencies along the axial direction (x-direction) and radial directions (y- and z-directions), showing (−0.16, 0.08, and 0.08) T/m/A in (x, y, z) directions with greater than 98% homogeneity within the receive chamber. Measured and simulated gradient efficiencies show excellent agreement.

were randomly rearranged within each group to eliminate any potential biases that may stem from system drift as well as to ensure repeatability. After each repetition sweeping all 25 OPs, the sample was physically removed from the receive chamber, and the temperatures of

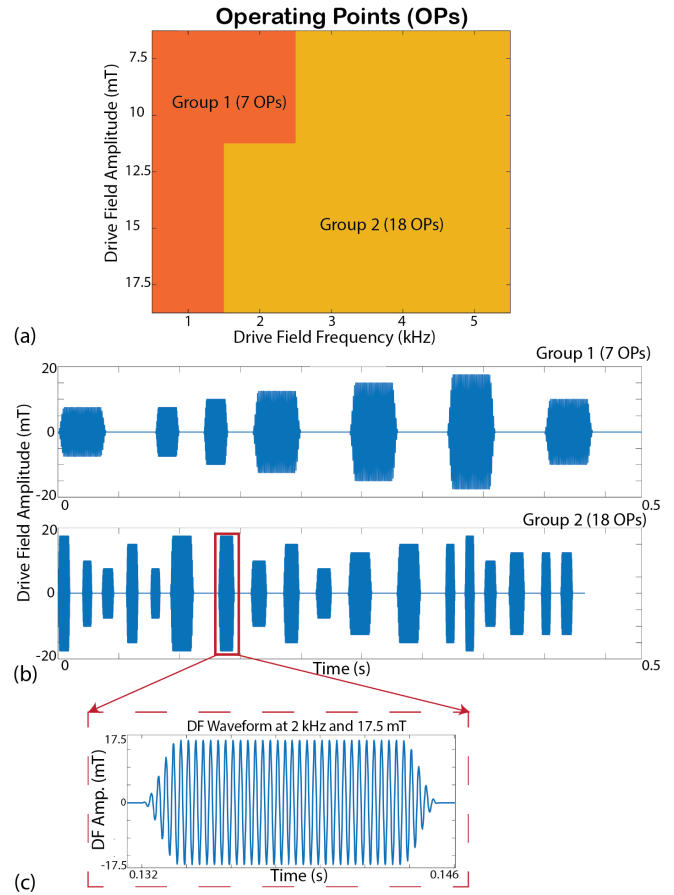


FIG. 2. (a) A total of 25 DF operating points (OPs) were divided into two groups with comparable signal strengths. (b) Example DF waveforms from the two groups, which had comparable total durations of approximately 450 ms. (c) A close-up view of the DF waveform from an example DF setting of 2 kHz and 17.5 mT.

both the sample and the receive chamber were monitored with a non-contact infrared thermometer (TFA SCANTEMP 330). No change in temperature was observed throughout the experiments. Note that temperature stability is crucial for these experiments, as temperature changes can introduce confounding effects on the results. Specifically, an increase in temperature can directly affect relaxation dynamics via altering the Brownian and Néel relaxation processes and indirectly by reducing viscosity, which further impacts the Brownian relaxation process.⁷

Samples were prepared at five different viscosity levels between 0.89 and 6.90 mPa s using varying ratios of water/glycerol mixtures, as listed in Table I.²⁷ This range covers the viscosity levels that are significant in a biological context.^{28,29} Each sample had a total volume of 140 μl and contained 65 μl of Perimag MNPs (c(Fe) = 8.5 mg/ml, Micromod GmbH). Placed in a flat-bottom 0.3 ml vial, the samples had an approximate size of 5.8 mm in diameter and 5.3 mm in height.

In the experiments, seven different SF gradients between $G = 0$ and 1.1 T/m were applied at each OP and for each sample. In total, 2625 measurements were performed (seven different SF gradients, five viscosity levels, 25 OPs, and three repetitions).

TABLE I. Viscosity levels (η) at 25 °C and composition for the nanoparticle samples. The added glycerol and water volumes and the final glycerol percentage by volume are listed. The total volume for each sample was 140 μ l, containing 65 μ l Perimag MNPs.

| η (mPa s) | Glycerol (μ l) | Water (μ l) | Glycerol (vol. %) |
|----------------|---------------------|------------------|-------------------|
| 0.89 | 0 | 75 | 0 |
| 1.73 | 28 | 47 | 20 |
| 2.58 | 42 | 33 | 30 |
| 4.07 | 56 | 19 | 40 |
| 6.90 | 70 | 5 | 50 |

The relaxation time constant was estimated using TAURUS as described in Eq. (4), utilizing eight periods of the acquired signal to increase estimation robustness.¹⁰ Since τ is expected to decrease with increasing DF frequency,³⁰ a normalization was performed as follows to enable comparison across different DF frequencies:

$$\hat{\tau} = \frac{\tau}{T_0} \times 100. \quad (5)$$

Here, $T_0 = 1/f_0$ is the period of the DF sinusoid and $\hat{\tau}$ is the percentage value of τ with respect to the DF period, which quantifies the relative delay in signal within one period.⁷

Figure 3 shows example results comparing MNP signals at a single OP at 1 kHz and 7.5 mT but at different SF gradients and viscosities. In Fig. 3(a), the signal amplitude decreases, and the width of the signal peak widens as the gradient is increased from 0 to 1.1 T/m at a constant viscosity of $\eta = 0.89$ mPa s. Despite this visible widening, the estimated $\hat{\tau}$ values were 3.02%, 3.45%, and 3.23% at 0, 0.7, and 1.1 T/m SF gradients, respectively, indicating a relatively stable trend in $\hat{\tau}$. In addition, the time difference between the positive and negative signal peaks gets shorter with increasing gradient, which potentially stems from a slight (approximately 5 mm) offset between the FFP and the center of the MNP distribution within the sample vial along the z -direction. Note that the smallest field-of-view (FOV) scanned by the FFP (for the case of the smallest DF amplitude and largest SF gradient) is approximately 27.3 mm, indicating that the FOV sufficiently covers the MNP sample in all cases. Importantly, this offset does not affect the relaxation time calculations, as TAURUS can be applied to both MPS and MPI signals.⁴

Figure 3(b) displays example MNP signals comparing low viscosity ($\eta = 0.89$ mPa s) vs high viscosity ($\eta = 6.90$ mPa s) cases at two different SF gradients of 0 and 1.1 T/m. The low viscosity case displays a reduced peak amplitude with slightly increased signal width. The estimated $\hat{\tau}$ for low vs high viscosity cases was 3.52% vs 3.48% at 0 T/m, and 2.02% vs 0.14% at 1.1 T/m. Accordingly, the high viscosity sample displays a significant reduction in $\hat{\tau}$ when the SF gradient is increased. While the signals at 1.1 T/m have visibly larger signal widths than those at 0 T/m, this widening did not yield larger $\hat{\tau}$ values at 1.1 T/m. This discrepancy stems from the fact that $\hat{\tau}$ indicates the deviation from mirror symmetry and not the widening in the signal peak.

Figure 4 displays the mean values of $\hat{\tau}$ at all OPs as color maps, for viscosity levels between 0.89 and 6.90 mPa s and SF gradients between 0 and 1.1 T/m. First, the overall trends in $\hat{\tau}$ are consistent with those in previous work:⁷ (1) $\hat{\tau}$ generally increases with DF frequency and decreases with DF amplitude, and (2) there is an abrupt increase

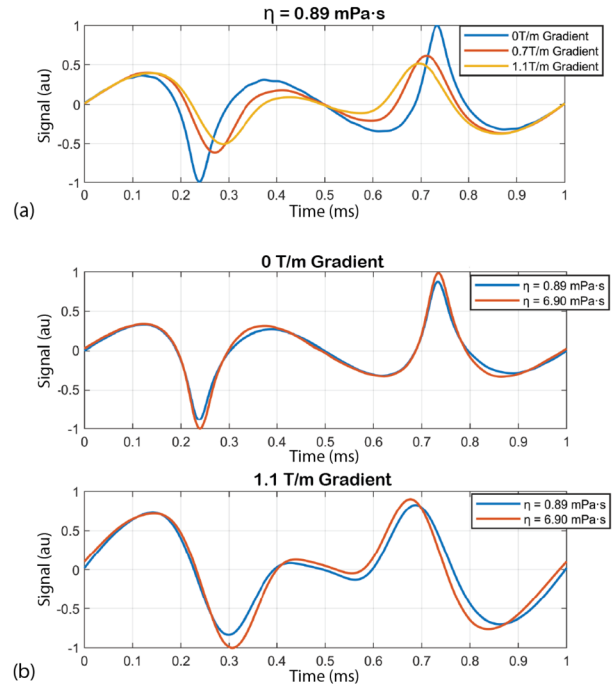


FIG. 3. Example measured signals at 1 kHz and 7.5 mT DF settings. (a) The measured signals for three different SF gradients for a fixed viscosity of $\eta = 0.89$ mPa s. (b) The measured signals for low viscosity ($\eta = 0.89$ mPa s) and high viscosity ($\eta = 6.90$ mPa s) cases at two different SF gradients of $G = 0$ and $G = 1.1$ T/m.

in $\hat{\tau}$ at $\eta = 0.89$ mPa · s at low DF amplitudes and frequencies. Interestingly, at the lowest DF amplitudes and frequencies (e.g., at 1 kHz and 7.5 mT), $\hat{\tau}$ suddenly falls down to very small values when

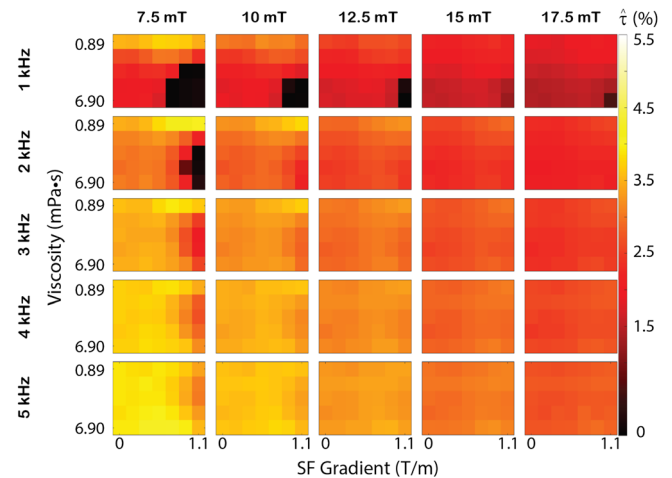


FIG. 4. Percentage relaxation time, $\hat{\tau}$, as functions of viscosity and SF gradient across 25 different operating points. The rows and columns display $\hat{\tau}$ as color maps at distinct DF frequencies and amplitudes ranging from 1 to 5 kHz and 7.5–17.5 mT, as indicated by the leftmost and topmost labels.

both the viscosity level and the SF gradient are increased. This trend suggests that at lower DF settings, relaxation of the highly viscous MNPs is significantly affected by the superimposed DC fields stemming from the SF gradients of MPI. One way to explain this phenomenon is to consider that the physical rotation in Brownian relaxation significantly slows down at higher viscosity levels, and therefore, the Néel relaxation becomes more dominant.³¹ It was shown that the Néel relaxation is significantly more sensitive to changes in the applied field when compared to the Brownian relaxation.³² Therefore, as the effective relaxation skews toward the Néel relaxation at high viscosity levels, the additional field of the SF gradients leads to drastic changes in $\hat{\tau}$.

In Fig. 5(a), a more detailed visualization of $\hat{\tau}$ as a function of SF gradient is plotted for different viscosity levels and DF amplitudes. A high degree of consistency is observed across the three repetitions. At high viscosity levels of $\eta \geq 2.85$ mPa·s, $\hat{\tau}$ gets smaller when the SF gradient is increased. This effect becomes increasingly more dominant at lower DF amplitudes and frequencies. Furthermore, this effect is observed at a lower SF gradient when the viscosity is higher. These changes in the behavior of MNPs with respect to viscosity and SF gradient suggest that SF gradients can be utilized to increase viscosity sensitivity in MPI.

The modulations in viscosity sensitivity can be better observed in Fig. 5(b), where we visualize $\hat{\tau}$ as a function of viscosity for all OPs. Figure 5(b) shows that viscosity sensitivity of $\hat{\tau}$ increases when the SF gradient is increased, and that this effect is more prominent for lower DF settings (i.e., lower DF amplitudes and frequencies). For example, at 1 kHz and 7.5 mT DF settings, $G = 0.7$ T/m suffices for sensitizing $\hat{\tau}$ to viscosity. At 1 kHz and 10 mT DF settings, a slightly larger SF gradient of $G = 0.9$ T/m can achieve a similar effect. In contrast, at the highest DF settings of 5 kHz and 17.5 mT, $\hat{\tau}$ shows a completely flat

response with respect to viscosity, and even $G = 1.1$ T/m is not sufficient to sensitize $\hat{\tau}$ to viscosity. Hence, the trends in Fig. 5(b) indicate that progressively larger SF gradients are needed to enhance viscosity sensitivity at higher DF frequencies and higher DF amplitudes.

Previous work has demonstrated that the widely popular DF frequencies around 25 kHz are not suitable for probing viscosity, since viscosity sensitivity falls down at high DF frequencies and amplitudes.^{8,18} This observation implies that viscosity mapping applications of MPI may need to be restricted to lower DF frequencies and amplitudes, where signal-to-noise ratio (SNR) is bound to be limited.³⁰ For example, the MPI signal at 1 kHz and 5 mT DF settings would yield approximately 50 times lower SNR than the MPI signal at 25 kHz and 10 mT, which is a massive difference. Therefore, boosting the viscosity sensitivity at DF settings that provide sufficient SNR is critical for MPI. Along these lines, a previous work has shown that a high viscosity sensitivity can be achieved on an MPI system with a relatively large SF gradient of $G = 4.8$ T/m at relatively high DF settings of 9.7 kHz and 25 mT.⁸ In contrast, on the same MPI system, $\hat{\tau}$ showed a flat response with respect to viscosity when the DF frequency was further increased to 26.3 kHz, implying that an even larger SF gradient was needed to attain viscosity sensitivity at this DF setting. In light of the trends demonstrated in Fig. 5(b), these results suggest that a large enough SF gradient can potentially sensitize $\hat{\tau}$ to viscosity even at high DF frequencies and amplitudes, which can enable high SNR without sacrificing viscosity sensitivity.

Apart from improving the viscosity sensitivity of MPI systems, magnetic field gradients can also be added to MPS systems for the detection of biomarkers such as antibodies. Utilizing MPS for point-of-care diagnostics is cheap, flexible, and fast. A previous method called COMPASS has shown that combining an MPS setup with a

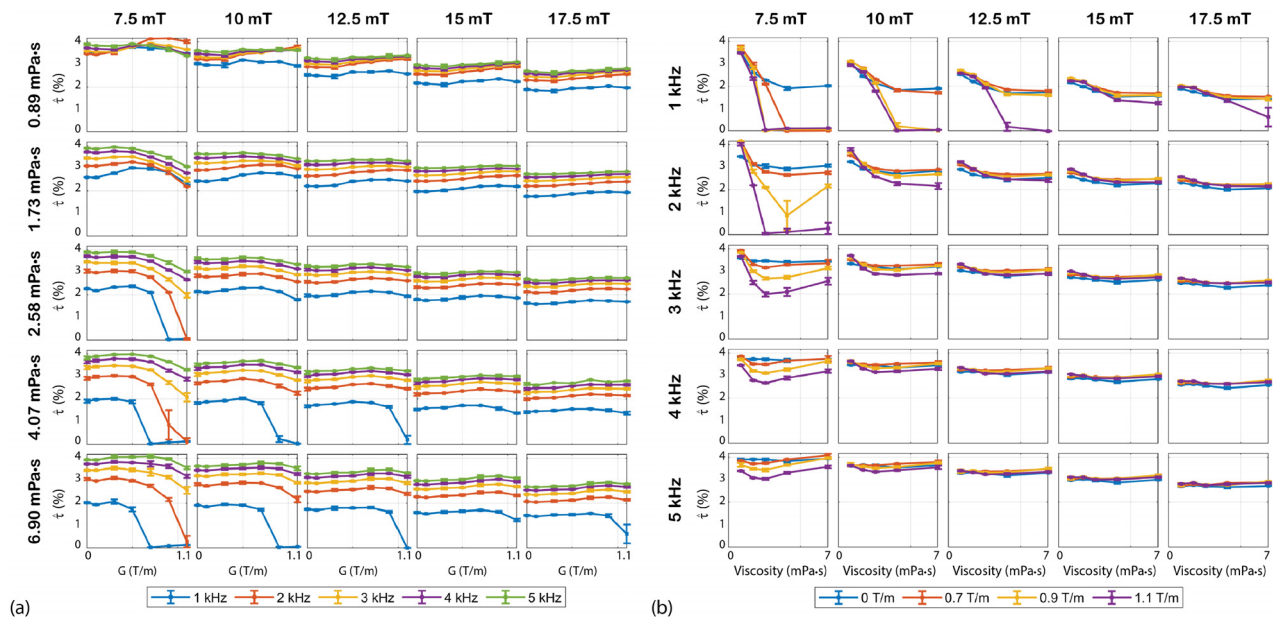


FIG. 5. (a) Percentage relaxation time, $\hat{\tau}$, with respect to the SF gradient displayed as line plots, where different colors correspond to different DF frequencies. The rows and columns display the results at distinct viscosity levels and DF amplitudes. (b) $\hat{\tau}$ with respect to the viscosity level displayed as line plots, where different colors correspond to different SF gradients. The rows and columns display the results at distinct DF frequencies and amplitudes. The error bars indicate standard deviations (STDs) across three repetitions.

critical offset DC field sensitizes the signal to changes in the mobility of MNPs, enabling the detection of SARS-CoV-2 antibodies binding to the functionalized MNPs.³³ That work has also demonstrated that applying a field gradient instead of a DC field offset substantially increases the differentiation sensitivity for binding states of MNPs. While that work did not provide a systematic analysis of the effect of the field gradient strength, its results are in agreement with our work, implying that stronger field gradients help increase viscosity/mobility sensitivity.³³

A potential challenge for viscosity mapping with MPI is the nonlinear relationship between τ and viscosity, as seen in Fig. 5(b) and reported in earlier studies.^{8,18} While a near-linear relationship is desirable for mapping application, the more fundamental requirement is to have a one-to-one relationship between τ and viscosity. The results of this work demonstrate that SF gradients can help establish such a one-to-one relationship. Once this requirement is achieved, a practical approach to address nonlinearity is to perform calibration experiments to determine the τ vs viscosity curve over a sufficiently wide range of viscosities (e.g., using point source samples prepared at varying viscosity levels). This calibration curve can then be used to convert τ maps into viscosity maps.

To summarize, this work demonstrates that utilizing SF gradients boosts the viscosity sensitivity in MPI. This approach can also be applied on an MPS setup equipped with additional field gradients for point-of-care diagnostic applications. In addition, particularly for MPI systems featuring DC electromagnet SF coils that allow SF gradients to be changed, this principle opens up a previously untapped parameter space for improving the functional imaging capabilities of MPI.

This work was supported by the Scientific and Technological Research Council of Turkey (TUBITAK 120E208, 122E162, and 22AG016/23AG005).

AUTHOR DECLARATIONS

Conflict of Interest

The authors have no conflicts to disclose.

Author Contributions

A. Topcu: Conceptualization (lead); Data curation (lead); Formal analysis (lead); Investigation (lead); Methodology (lead); Software (lead); Visualization (lead); Writing – original draft (equal); Writing – review & editing (equal). **A. Alpman:** Data curation (supporting); Formal analysis (supporting); Methodology (supporting); Software (supporting); Writing – review & editing (supporting). **M. Utkur:** Conceptualization (supporting); Formal analysis (supporting); Methodology (supporting); Software (supporting); Writing – original draft (supporting); Writing – review & editing (supporting). **E. U. Saritas:** Conceptualization (equal); Funding acquisition (lead); Investigation (equal); Project administration (lead); Resources (lead); Supervision (lead); Writing – original draft (equal); Writing – review & editing (equal).

DATA AVAILABILITY

The data that support the findings of this study are available from the corresponding authors upon reasonable request.

REFERENCES

- B. Gleich and J. Weizenecker, *Nature* **435**, 1214–1217 (2005).
- J. Weizenecker, J. Borgert, and B. Gleich, *Phys. Med. Biol.* **52**, 6363 (2007).
- L. R. Croft, P. W. Goodwill, and S. M. Conolly, “Relaxation in X-space magnetic particle imaging,” *IEEE Trans. Med. Imaging* **31**, 2335–2342 (2012).
- Y. Muslu, M. Utkur, O. B. Demirel, and E. U. Saritas, “Calibration-free relaxation-based multi-color magnetic particle imaging,” *IEEE Trans. Med. Imaging* **37**, 1920–1931 (2018).
- C. Stehning, B. Gleich, and J. Rahmer, “Simultaneous magnetic particle imaging (MPI) and temperature mapping using multi-color MPI,” *Int. J. Magn. Part. Imaging* **2**, 1612001 (2016).
- J. Wells, H. Paysen, O. Kosch, L. Trahms, and F. Wiekhorst, “Temperature dependence in magnetic particle imaging,” *AIP Adv.* **8**, 056703 (2018).
- M. Utkur and E. U. Saritas, “Simultaneous temperature and viscosity estimation capability via magnetic nanoparticle relaxation,” *Med. Phys.* **49**, 2590–2601 (2022).
- M. Utkur, Y. Muslu, and E. U. Saritas, “Relaxation-based color magnetic particle imaging,” *Appl. Phys. Lett.* **115**, 152403 (2019).
- J. Rahmer, A. Halkola, B. Gleich, I. Schmale, and J. Borgert, “First experimental evidence of the feasibility of multi-color magnetic particle imaging,” *Phys. Med. Biol.* **60**, 1775 (2015).
- M. T. Arslan, A. A. Özarslan, S. Kurt, Y. Muslu, and E. U. Saritas, “Rapid TAURUS for relaxation-based color magnetic particle imaging,” *IEEE Trans. Med. Imaging* **41**, 3774–3786 (2022).
- W. L. Chandler and G. Schmer, “Evaluation of a new dynamic viscometer for measuring the viscosity of whole blood and plasma,” *Clin. Chem.* **32**, 505–507 (1986).
- G. Deliconstantinos, V. Villiotou, and J. C. Stavrides, “Increase of particulate nitric oxide synthase activity and peroxynitrite synthesis in UVB-irradiated keratinocyte membranes,” *Biochem. J.* **320**(3), 997–1003 (1996).
- C. Shasha, E. Teeman, and K. M. Krishnan, “Harmonic simulation study of simultaneous nanoparticle size and viscosity differentiation,” *IEEE Magn. Lett.* **8**, 1509405 (2017).
- A. M. Rauwerdink and J. B. Weaver, “Harmonic phase angle as a concentration-independent measure of nanoparticle dynamics,” *Med. Phys.* **37**, 2587–2592 (2010).
- J. B. Weaver, A. M. Rauwerdink, and E. W. Hansen, “Magnetic nanoparticle temperature estimation,” *Med. Phys.* **36**, 1822–1829 (2009).
- M. Möddel, C. Meins, J. Dieckhoff, and T. Knopp, “Viscosity quantification using multi-contrast magnetic particle imaging,” *New J. Phys.* **20**, 083001 (2018).
- S. Draack, M. Schilling, and T. Viereck, “Magnetic particle imaging of particle dynamics in complex matrix systems,” *Phys. Sci. Rev.* **8**, 213–237 (2023).
- M. Utkur, Y. Muslu, and E. U. Saritas, “Relaxation-based viscosity mapping for magnetic particle imaging,” *Phys. Med. Biol.* **62**, 3422 (2017).
- P. W. Goodwill and S. M. Conolly, “The X-space formulation of the magnetic particle imaging process: 1-D signal, resolution, bandwidth, SNR, SAR, and magnetostimulation,” *IEEE Trans. Med. Imaging* **29**, 1851–1859 (2010).
- T. Knopp and T. M. Buzug, *Magnetic Particle Imaging: An Introduction to Imaging Principles and Scanner Instrumentation* (Springer-Verlag, Berlin, Heidelberg, 2012), pp. 1–204.
- W. F. Brown, “Thermal fluctuations of a single-domain particle,” *Phys. Rev.* **130**, 1677 (1963).
- L. Néel, “Théorie du trainage magnétique des ferromagnétiques en grains fins avec application aux terres cuites,” *Ann. Géophys.* **5**, 99–136 (1949).
- Z. W. Tay, P. W. Goodwill, D. W. Hensley, L. A. Taylor, B. Zheng, and S. M. Conolly, “A high-throughput, arbitrary-waveform, MPI spectrometer and relaxometer for comprehensive magnetic particle optimization and characterization,” *Sci. Rep.* **6**, 34180 (2016).
- A. Alpman, M. Utkur, and E. U. Saritas, “MNP characterization and signal prediction using a model-based dictionary,” *Int. J. Magn. Part. Imaging* **8**, 2203017 (2022).
- B. Kilic, D. A. Soydan, A. Güngör, and C. B. Top, “Inverse radon transform-based reconstruction with an open-sided magnetic particle imaging prototype,” *Signal, Image Video Process.* **17**, 1563 (2023).
- J. Franke, N. Baxan, H. Lehr, U. Heinen, S. Reinartz, J. Schnorr, M. Heidenreich, F. Kiessling, and V. Schulz, “Hybrid MPI-MRI system for dual-modal in situ cardiovascular assessments of real-time 3D blood flow

- quantification—A pre-clinical in vivo feasibility investigation,” *IEEE Trans. Med. Imaging* **39**, 4335–4345 (2020).
- ²⁷N. S. Cheng, “Formula for the viscosity of a glycerolwater mixture,” *Ind. Eng. Chem. Res.* **47**, 3285–3288 (2008).
- ²⁸M. K. Kuimova, S. W. Botchway, A. W. Parker, M. Balaz, H. A. Collins, H. L. Anderson, K. Suhling, and P. R. Ogilby, “Imaging intracellular viscosity of a single cell during photoinduced cell death,” *Nat. Chem.* **1**, 69–73 (2009).
- ²⁹K. Bera, A. Kiepas, I. Godet, Y. Li, P. Mehta, B. Ifemembi, C. D. Paul, A. Sen, S. A. Serra, K. Stoletov, J. Tao, G. Shatkin, S. J. Lee, Y. Zhang, A. Boen, P. Mistriotis, D. M. Gilkes, J. D. Lewis, C. M. Fan, A. P. Feinberg, M. A. Valverde, S. X. Sun, and K. Konstantopoulos, “Extracellular fluid viscosity enhances cell migration and cancer dissemination,” *Nature* **611**, 365–373 (2022).
- ³⁰L. R. Croft, P. W. Goodwill, J. J. Konkle, H. Arami, D. A. Price, A. X. Li, E. U. Saritas, and S. M. Conolly, “Low drive field amplitude for improved image resolution in magnetic particle imaging,” *Med. Phys.* **43**, 424 (2015).
- ³¹A. L. Andrade, L. C. D. Cavalcante, J. D. Fabris, M. C. Pereira, L. E. Fernandez-Outon, D. C. Pedersoli, J. D. Ardisson, R. Z. Domingues, and J. M. Ferreira, “Magnetically induced heating by iron oxide nanoparticles dispersed in liquids of different viscosities,” *Ceram. Int.* **46**, 21496–21504 (2020).
- ³²R. J. Deissler, Y. Wu, and M. A. Martens, “Dependence of Brownian and Néel relaxation times on magnetic field strength,” *Med. Phys.* **41**, 012301 (2014).
- ³³P. Vogel, M. A. Rückert, B. Friedrich, R. Tietze, S. Lyer, T. Kampf, T. Hennig, L. Dölken, C. Alexiou, and V. C. Behr, “Critical offset magnetic particle spectroscopy for rapid and highly sensitive medical point-of-care diagnostics,” *Nat. Commun.* **13**, 7230 (2022).